第４回地震時保有耐力法に基づく橋梁の耐震設計
に関するシンポジウム講演論文集 (2000年12月)

MODELING OF THREE-DIMENSIONAL POUNDING OF BRIDGE GIRDERS

Ping ZHU[1], Masato ABE[2], Yozo FUJINO[3]

[1]Student member, Ph. D. Candidate Zhu@bridge.t.u-tokyo.ac.jp
[2]Member, Associate Professor, Masato@bridge.t.u-tokyo.ac.jp
[3]Fellow, Professor Fujino@bridge.t.u-tokyo.ac.jp

Department of Civil Engineering, University of Tokyo 7-3-1 Hongo, Bunkyo-Ku, Tokyo 113-8656, Japan

Abstract

A model is presented for three-dimensional pounding problems with friction. The contacting surfaces are assumed to be planes and penetrations of contactor nodes to target surfaces are allowed and utilized for computing pounding reactions. The rules of relative surface displacements are imposed directly to satisfy the compatibility conditions of contacting bodies. On considering the pounding problems of bridge girders under earthquakes, the paper implements the model in a general-purpose dynamic analysis program for bridges. Experiments of pounding have also been conducted for verifying this model. The applicability of the model is illustrated by selected results of experiments and computations.

Introduction

Unseating of bridge girders/decks during earthquakes is strongly harmful to the usability of bridges. Evidence shows that in addition to damage along longitudinal direction, lateral displacement of bridge girders caused by pounding can also lead to the damage of unseating. To take into account of this effect in analysis, a 3D model of pounding between girders is needed.

Several solution methods are available for contact/pounding problems. According to problems oriented, the methods can be categorized into two main groups as follow:

(1) capable of arbitrary contact of bodies/surfaces: In Reference 1, a solution method of 3D contact problems with friction has been presented based on Lagrange multiplier technique. The merit of this method is that it can be applied to a wide range of static and dynamic problems with material and geometric non-linearities. Relatively complicated algorithm is a demerit. Moreover, the method is unsuitable to be used directly to a system composed of bar elements.

(2) to deal with pounding of two prescribed points: A method for point-to-point pounding problem of buildings using Lagrange multiplier method is given in Reference 2. Post-contact conditions of impulse-momentum relationship have been discussed in this paper. Reference 3 gives an approach for point-to-point pounding in buildings on considering energy loss during impact. The same method has been used for analysis of pounding between bridge girders in Reference 5. A method for pounding between two adjacent bridge segments by applying the law of conservation of momentum and energy directly to post-pounding conditions is also presented in Reference 4. Among this group of method, clear physical meaning and simple algorithm are merits. The main demerit is that 3D arbitrary contact cannot be simulated.

As the common adopted method for pounding between girders is to use contact elements, which is for 1D fixed point-to-point case, a 3D contact-friction model for the pounding problem has been developed by this paper.

3D contact-friction model for pounding

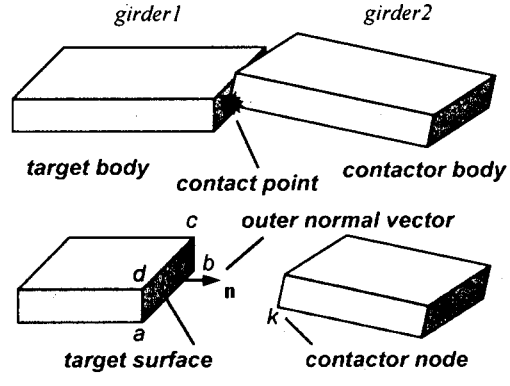

Fig. 1 Bridge girders in arbitrary contact

The problem considered herein is a general case of pounding by two bridge girders. As shown in Fig. 1, two girders contact with each other arbitrarily. They are referred as contactor body and target body where a contact happens between contactor node and target surface.

A 3D contact-friction model for the problem is illustrated in Fig. 2. The target surface, named as *abcd*, is assumed as a rigid plane (The surface is not necessary to be a rectangle). *OXYZ* is the inertial coordinate system. Vector **n** is the outer normal vector of the target surface. Node *k* is the contactor node at the contactor body, which penetrates into the target surface during contact. Point *p* is the physical contact point at the target surface *abcd*.

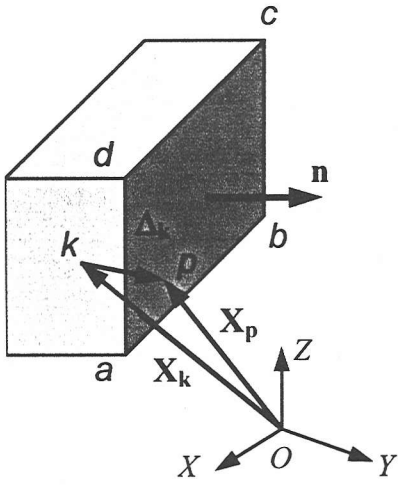

(a) Sketch of the model

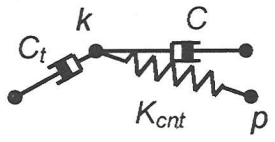

(b) Spring and dashpots applied to node k during contact

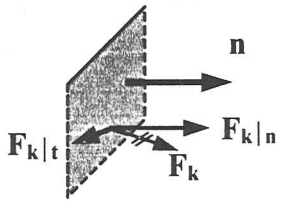

(c) Contact force at node k by the universal spring

Fig. 2 Illustration of the 3D contact-friction model

During contact the position and velocity at point *p* are functions of the target surface, which can be described in eqn. (1) and (2). The material overlaps at node *k*, Δ_k, and the relative velocity of node *k* to point *p*, $\mathbf{V}_{kp}$, can be calculated by eqn. (3) and (4) respectively.

$$\mathbf{p} = \mathbf{p}(\mathbf{a}, \mathbf{b}, \mathbf{c}, \mathbf{d}) \tag{1}$$

$$\mathbf{V}_p = \mathbf{V}_p(\mathbf{V}_a, \mathbf{V}_b, \mathbf{V}_c, \mathbf{V}_d) \tag{2}$$

$$\Delta_k = \mathbf{X}_p - \mathbf{X}_k \tag{3}$$

$$\mathbf{V}_{kp} = \mathbf{V}_k - \mathbf{V}_p \tag{4}$$

The model utilizes material penetrations to compute forces during contact. Upon contact, a universal spring K_{cnt} between node *k* and point p is created to compute the force of contact. Two dashpots, *C* and C_t, are also applied to node *k* for simulating energy loss during contact (See Fig. 2(b)). The contact force at node *k*, $\mathbf{F}_k$, can be computed by eqn. (5) and be divided into normal and tangent components ($\mathbf{F}_k|_n$ and $\mathbf{F}_k|_t$ respectively) as eqn. (6), where vector **n** is the outer normal vector of the target surface and vector **t** is a projection vector of $\mathbf{F}_k$ to the target surface. (See Fig. 2(c)).

$$\mathbf{F}_k = K_{cnt} \cdot \Delta_k \tag{5}$$

$$\mathbf{F}_k = \mathbf{F}_k|_n + \mathbf{F}_k|_t \tag{6}$$

Status of contact

The relative position between contactor node *k* and target surface *abcd* is utilized to identify a contact. The inside and outside of the target body is determined by **n**, the outer normal vector of the plane, which indicates the outer direction of the target body (See Fig. 2(a)). A contact happens when the contactor node *k* passes through (goes inside the target body) the target surface and ends when node *k* moves out of the surface (outside). During contact, status can be divided into stick contact and slide contact. The condition of stick and slide contact is decided by the ratio of tangent component of the contact force $|\mathbf{F}_k|_t|$ to the normal one $|\mathbf{F}_k|_n|$ (eqn. (7a), (7b)). The idea is illustrated by Fig. 3. A cone shows the maximum static friction the target surface can supply according to the normal force. If the contact force vector is inside the cone, the relative movement between the node and the surface is prevented due to friction force. Therefore the node sticks to the surface during contact. Otherwise, slide will happen.

Stick condition: $$\left|\mathbf{F}_k|_t\right| < \mu_s \left|\mathbf{F}_k|_n\right| \tag{7a}$$

Slide condition: $$\left|\mathbf{F}_k|_t\right| \geq \mu_s \left|\mathbf{F}_k|_n\right| \tag{7b}$$

μ_s - static friction coeff.

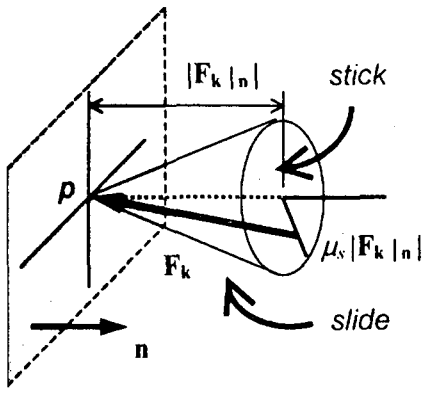

Fig. 3 Condition to decide status of stick and slide

Constraints on surface displacements due to contact

Geometrical compatibility conditions must be satisfied when two bodies come into contact. The conditions of constraints for stick and slide contact are illustrated with Fig. 4. In case of stick contact, node k will move towards point p as the action of the universal spring K_{cnt} (which is set between k and p); in slide contact, in additional to the component of movement towards point p, node k will have a trend to move within a plane inside and parallel to the target surface. As a consequence of slide, the physical contact point p will be updated to point p' in accordance with the new position of node k, k', by projecting k' to the target surface.

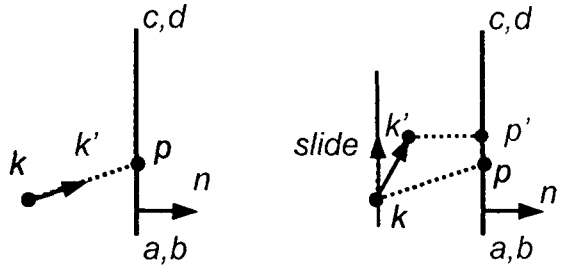

(a) In case of stick contact (b) In case of slide contact

Fig. 4 Constraints on displacements

Contact forces at contactor node

Contact forces are calculated separately for stick and slide conditions. As shown in eqn. 8, in the case of stick contact, the force at node k, $\mathbf{R}_k$, consists of the contact force $\mathbf{F}_k$ (by spring K_{cnt}) which is given by eqn. (5) and damping forces at normal and tangent directions $\mathbf{F}_c|_n$ and $\mathbf{F}_c|_t$ (by dashpots C and C_t) according to eqn. (9a) and (9b). In slide condition, the force $\mathbf{R}_k$ is composed with the normal component of contact force $\mathbf{F}_k|_n$, normal damping force $\mathbf{F}_c|_n$ and kinetic friction $\mathbf{F}_f|_t$ at tangent direction. $\mathbf{F}_f|_t$ is given in eqn. (9c) and its direction is at the reverse way of the tangent component of relative velocity $\mathbf{V}_{kp}$.

Stick condition: $$\mathbf{R}_k = \mathbf{F}_k + \mathbf{F}_c|_n + \mathbf{F}_c|_t \quad (8a)$$

Slide condition: $$\mathbf{R}_k = \mathbf{F}_k|_n + \mathbf{F}_c|_n + \mathbf{F}_f|_t \quad (8b)$$

$$\mathbf{F}_c|_n = -C \cdot \mathbf{V}_{kp}|_n \quad (9a)$$

$$\mathbf{F}_c|_t = -C_t \cdot \mathbf{V}_{kp}|_t \quad (9b)$$

$$\mathbf{F}_f|_t = -\mu_k \cdot |\mathbf{F}_k|_n| \frac{\mathbf{V}_{kp}|_t}{|\mathbf{V}_{kp}|_t|} \quad (9c)$$

μ_k - kinetic friction coeff.

Contact forces at target surface

Contact forces at target surface are obtained by applying the force at the contactor node to the target surface. As shown in Fig. 5, the forces are composed of forces at the four corners of the quadrilateral (eqn. (10)). The contact forces at the target surface are given by eqn. (11), where [T] is a distributed matrix by linear interpolation according to static equilibrium.

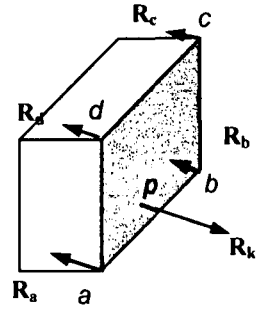

Fig. 5 Contact forces at target surface

$$\mathbf{R}_{target\_surface} = \begin{Bmatrix} \mathbf{R}_a \\ \mathbf{R}_b \\ \mathbf{R}_c \\ \mathbf{R}_d \end{Bmatrix} \quad (10)$$

$$\mathbf{R}_{target\_surface} = [\mathbf{T}](-\mathbf{R}_k) \quad (11)$$

Governing equations of motion

To apply the model to dynamic time-history analysis, incremental equilibrium equation of motion for iteration (i) at time t+Δt is as follow:

$$\mathbf{M}\Delta\ddot{\mathbf{U}}^{(i)} + \mathbf{C}\Delta\dot{\mathbf{U}}^{(i)} + {}^{t+\Delta t}\mathbf{K}\Delta\mathbf{U}^{(i)} = {}^{t+\Delta t}\mathbf{R} - \mathbf{M}^{t+\Delta t}\ddot{\mathbf{U}}^{(i-1)} - \mathbf{C}^{t+\Delta t}\dot{\mathbf{U}}^{(i-1)} - {}^{t+\Delta t}\mathbf{F}^{(i-1)} + {}^{t+\Delta t}\mathbf{R}_{cnt}^{(i-1)} \quad (12)$$

where

M, C, K – mass, damping and stiffness matrices respectively,

$\Delta\ddot{\mathbf{U}}^{(i)}, \Delta\dot{\mathbf{U}}^{(i)}, \Delta\mathbf{U}^{(i)}$ – incremental vectors of accelerations, velocities and displacements at iteration (i) respectively,

${}^{t+\Delta t}\ddot{\mathbf{U}}^{(i-1)}, {}^{t+\Delta t}\dot{\mathbf{U}}^{(i-1)}$ – vectors of accelerations and velocities after iteration (i-1) respectively,

${}^{t+\Delta t}\mathbf{R}$ – external load vector at time t+Δt,

${}^{t+\Delta t}\mathbf{F}^{(i-1)}$ – restoring force vector after iteration (i-1),

${}^{t+\Delta t}\mathbf{R}_{cnt}^{(i-1)}$ – vector of contact forces after iteration (i-1).

The vector of contact forces $\mathbf{R}_{cnt}$ is obtained with eqn. (13) and (14) by summating contact forces of all contact pairs, where a contact pairs consists of a contactor node and corresponding nodes on target surface.

$$\mathbf{R}_{cnt} = \sum_k \mathbf{R}_{cnt}|_k \tag{13}$$

$$\mathbf{R}_{cnt}|_k = \begin{Bmatrix} \mathbf{R}_k \\ \mathbf{R}_{target\_surface} \end{Bmatrix} = \begin{Bmatrix} \mathbf{R}_k \\ \mathbf{R}_a \\ \mathbf{R}_b \\ \mathbf{R}_c \\ \mathbf{R}_d \end{Bmatrix} \tag{14}$$

Parameters of the model

Parameters of the model are chosen as follow:

The axial stiffness of the contactor body can be used as the stiffness of the universal spring K_{cnt}. As presented in eqn. (15):

$$K_{cnt} = \frac{EA}{L} \tag{15}$$

where E, A and L are modulus of elasticity, cross section area and length of the contactor element respectively.

The damping ratio C and C_t can be determined according to the restitution coefficient at normal and tangent directions by eqn. (16) and (17).

$$C = 2\xi\sqrt{K_{cnt}\frac{M_1 M_2}{M_1 + M_2}} \tag{16}$$

$$\xi = \frac{-\ln e}{\sqrt{\pi^2 + (\ln e)^2}} \tag{17}$$

where,

M_1, M_2 – masses of the two bodies in contact

K_{cnt} – stiffness of the universal spring

e – restitution coefficient

ξ – damping ratio according to restitution coefficient e

The range of restitution coefficient is between 1 and 0, which represents the pounding from elastic to plastic. The corresponding range of ξ is between 0 and 1.

Verifications of the model

To ensure the applicability of the model, theoretical and experimental verifications have been conducted.

Theoretical verification

A test of adjacent rods with point masses on free vibration was selected. In the test (referred as test1) an initial displacement, which is given to point mass *m1*, starts free vibration of these two masses where energy is transferred in between as pure elastic impacts (see Fig. 6). Theoretical solution of the problem is shown in Fig. 7. To conduct an analysis, parameters of the model were chosen as Fig. 6. Two time intervals were used for time-history analysis. Results in Fig. 8. show that the accuracy of solution can be obtained by choosing small time interval.

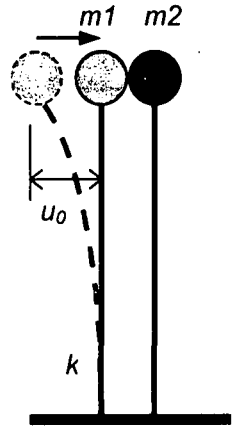

m1=m2=2 (kg)
ω=10.25 (rad/s)
$k=m\omega^2=210.125$ (N/m)
$u_0=0.1$ (m)

Parameters:
$K_{cnt}=1.5474\times10^5$ (N/m)
$C=C_t=0$
Δt= 0.002,
0.0001 (s)

Fig. 6 test1 - two point masses on free vibration

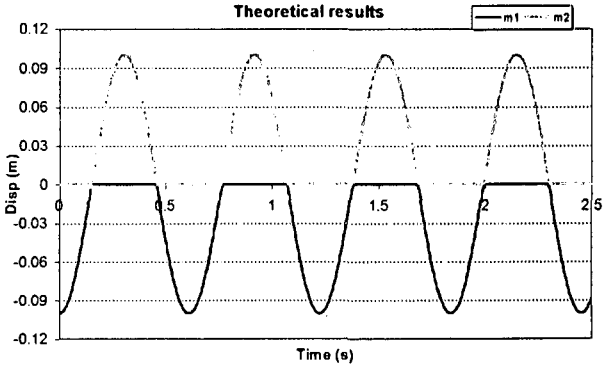

Fig. 7 test1 – theoretical solution (displ. of masses)

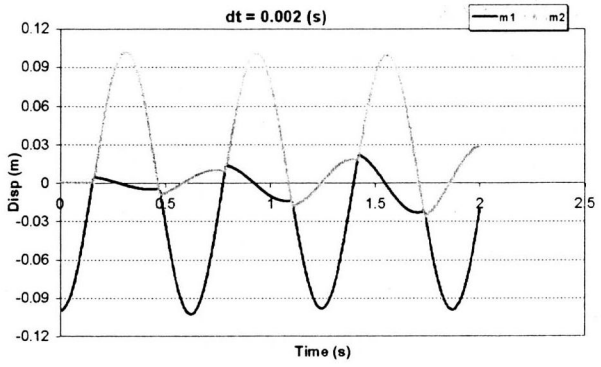

(a) Δt=0.002s

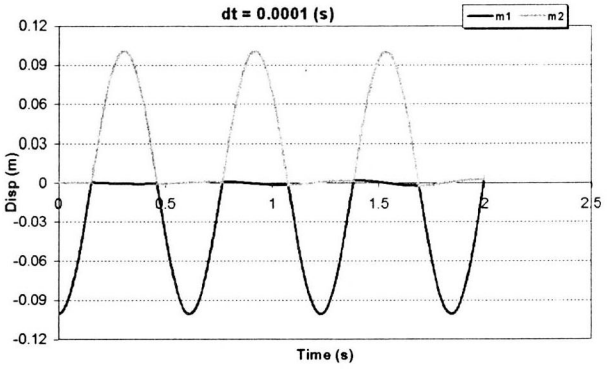

(b) Δt=0.0001s

Fig. 8 test1 – analytical results

Experimental verifications

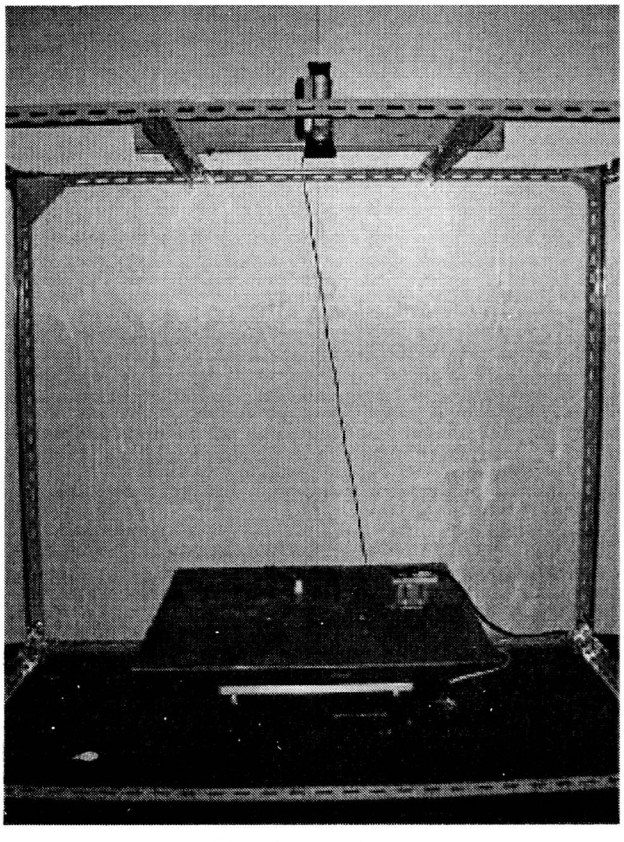

Fig. 9 the experiments

Experiments have also been conducted to verify the model in more complicated 2D cases [6]. Fig. 9 shows the method to conduct the experiments. A video camera is used to measure displacements of the model girder (three components in 2D) using image processing techniques. Fig. 10 shows a case of the experiments with one model girder, which is supported by rubber supports, and an abutment on a shaking table. The experiments (referred as test2) were taken in 1D and 2D cases according to the angle of excitation.

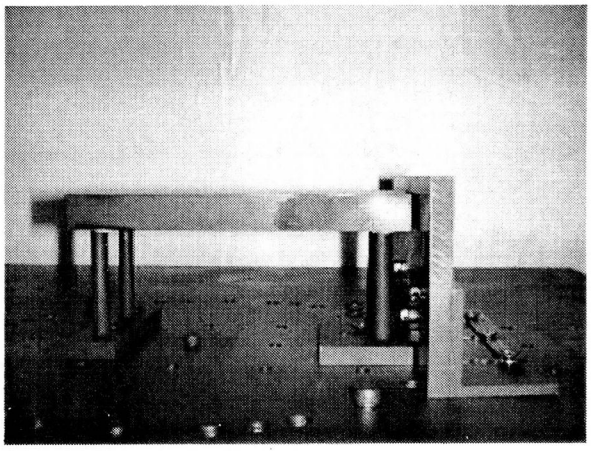

Fig. 10 test2 - pounding between model girder and abutment

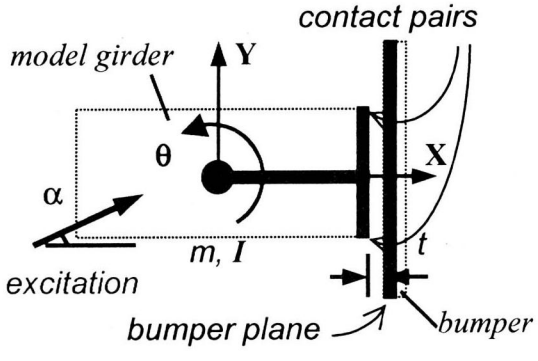

Fig. 11 test2 – analytical model

Data for computation are as follow:

m=2 (kg), $I=6.8\times10^{-3}$ (kgm^2), $K_{cnt}=1.5474\times10^5$ (N/m), C= 220.287 (Ns/m) (as e=0.4), C_t=26.3558 (Ns/m) (as e_t=0.9), μ_s=0.2, μ_k=0.15, α=22.5° (in 2D case); Δt=0.001 (s), excitations: sine waves.

Fig. 11 illustrates an analytical model of the experiments. The mass and rotational inertia of the model girder are concentrated at its center. Dimensions of the girder are simulated with rigid bars in "T" shape. To compute the effects of pounding, two contact pairs are placed in the analytical model.

Comparisons of experimental data and analytical results are given in Fig. 12 and Fig. 13 for 1D and 2D cases, respectively. Results of pounding can be seen from these figures. Agreements are good in translating displacements and relatively good in rotating displacement.

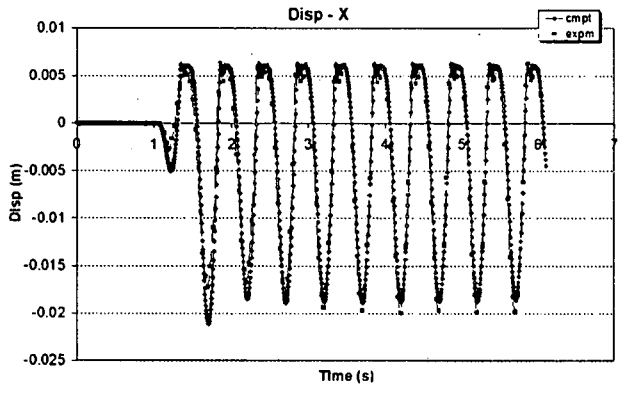

Fig. 12 test2 (1D case) – result comparison

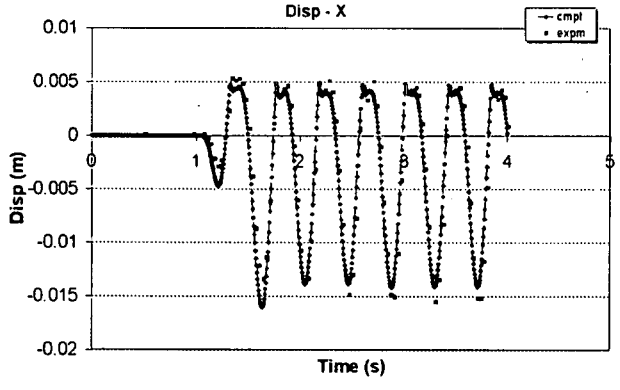

(a) X direction

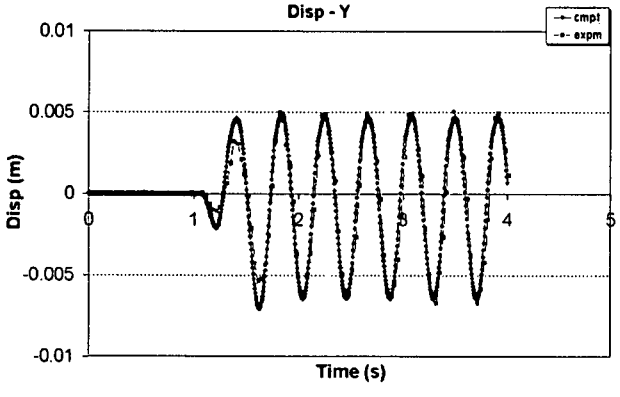

(b) Y direction

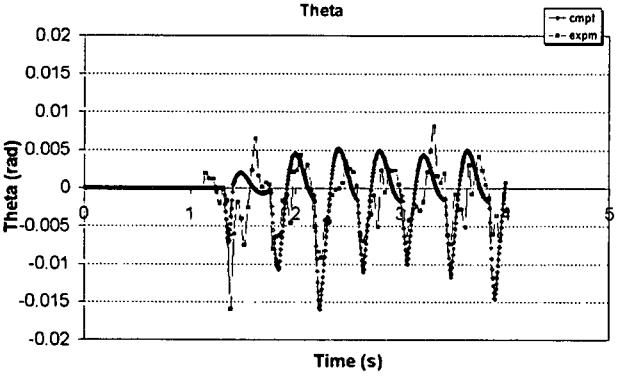

(c) rotating angle

Fig. 13 test2 (2D case) – result comparison

Conclusions

A 3D contact-friction model has been presented in this paper. On considering the pounding problem between bridge girders, an algorithm for solution has been developed. Theoretical verifications (in 1D case) and experimental verifications (a model girder and an abutment in 2D case) have also been conducted. The applicability of the model can be seen from the results of computations. This model is easy to be combined with the commonly used methods of time integration and is capable of dealing with the pounding problems between bridge girders.

Reference

1) Chaudhary A. B. and Bathe K. J., A solution method for static and dynamic analysis of three-dimensional contact problems with friction, *Computers & Structures* EERC 73-12Vol. 24, No. 6, pp. 855-873, 1986
2) Papadrakakis M., Mouzakis H., Plevris N. and Bitzarakis S., A lagrange multiplier solution method for pounding of buildings during earthquakes, *Earthquake Engineering and Structural Dynamics*, Vol. 20, pp. 981-998 1991
3) Anagnostopoulos S. A., Pounding of buildings in series during earthquakes, *Earthquake Engineering and Structural Dynamics*, Vol. 16, 443-456 1988
4) Ruangrassamee A. and Kawashima K., Relative displacement response spectra with pounding effect, *Proceedings of the First International Summer Symposium*, International Activities Committee JSCE, Tokyo, Japan, pp. 9-12, 1999
5) Jankowski R., Pounding of superstructure segments in elevated bridges during earthquakes and reduction of its effects, *Doctor's dissertation*. The University of Tokyo, 1997
6) 柳野和也, 橋梁の地震時桁間衝突現象のモデル化 (Modeling of Pounding Behavior of Bridge Girders under Seismic Excitations), *Master's thesis* , The University of Tokyo, 2000